encit 2020

ABCM Associação Brasileira de Engenharia e Ciências Mecânicas

18th Brazilian Congress of Thermal Sciences and Engineering
November 16-20, 2020 (Online)

ENC-2020-0331
NUMERICAL SIMULATION OF HYDRAULIC CONVEYING THROUGH A NARROW ELBOW

Elmar Anton Schnorr Filho
elmar.aschnorr@gmail.com
Nicolao Cerqueira Lima
nicolaol@hotmail.com
Erick de Moraes Franklin
franklin@fem.unicamp.br
School of Mechanical Engineering, University of Campinas - UNICAMP, Rua Mendeleyev, 200, Campinas, SP, Brazil

Abstract. *This work investigates the hydraulic transport of solid particles with d = 6 mm flowing in a narrow elbow with 25.4 mm-ID. The pipe consists of a horizontal section with a length of 3D, an elbow with a radius of 2D and a vertical section with a length of 5D. Elbows are ubiquitous in industrial pipelines and are subjected to erosion and blockage in the presence of solid particles. To access particles behavior, it was used a resolved CFD-DEM method, which combines the computational fluid dynamic (CFD) and the discrete element method (DEM). Particles were inserted at a constant mass rate and fluid was inserted at a constant velocity. The behavior of this solid-fluid flow was investigated.*

Keywords: *immersed boundary method, CFD-DEM, narrow pipe, elbow*

1. INTRODUCTION

Particulate materials are very relevant in human life, for they appear in different forms, like powders, grains and sands, covering more than 10% of Earth's surface. A few examples of granular materials are: coal, gravel, agricultural products (e.g. rice, soy, beans), chemical and pharmaceutical products like inks and pigments. Such materials are so bountiful that their processing corresponds to almost 10% of all energy spent in the world, standing just behind water in a scale of importance in human life (Duran, 2012). Flows combining solids and fluids can be seen in nature, for example, in river beds, in the defrosting of a glacier or in the formation of dunes in deserts. Not only they appear together in nature but also in industry. The relevance of both materials leads, naturally, to the development of processing techniques. For decades hydraulic conveying of solid particles has been used in mining, chemical and food industries and consists of using a fluid, specifically water, flowing along a pipeline and taking advantage of drag forces in to drive particles to a desired location (Uzi and Levy, 2018). It is a viable and efficient alternative to trucks and rails for transporting continuously high amounts of commodities, like coal, bitumen, ores and grains. It also could be employed in processing plants to quickly transport these raw materials between different locations. However these raw products appear in a broad range of sizes, shapes and physical properties, and pipelines may have complex geometries with elbows and tees, making the design of hydraulic conveying systems complex due to high amount of control variables and parameters, and the prediction of flow pattern, pressure drop or friction loss inside these pipes is a challenge (Vaezi *et al.*, 2018; Zhou *et al.*, 2019).

The presence of solid particles inside pipes may lead to undesirable, yet unavoidable, phenomena like erosion, which if not controlled can evolve to leaks, failures and potential injuries (Parsi *et al.*, 2014; Li *et al.*, 2019). In constrictions, particles can form stable bridges or arches, impeding other particles to flow and causing pressure buildup upstream (Parry and Millet, 2010; Mondal *et al.*, 2016). Particle deposition may happen if particles density is greater than the fluid density, leading to a heterogeneous flow and, if the flow rate is not large enough, also can cause blockages and solid backflow for inclined pipes, damaging the whole system (Zhou *et al.*, 2019). Moreover, elbows and tees are ubiquitous elements in pipelines and its abruptly change flow direction make them more susceptible to erosion due to particle impact. For that reason, it is essential and necessary to study the physics around particles flows in order to provide guidance to develop strategies, to avoid flow problems and to better control the process (Zhou *et al.*, 2010). Throughout years, several studies have been developed to describe and predict flow characteristics based on control variables, like fluid flow rate or solid density. Due to the complex nature of the problem, the former were in the form of empirical correlations and constructions of flow maps. But these correlations are restricted to specific setups and, therefore, incapable of extrapolating results to others configurations. Besides, their main focus is on pressure drop predictions or the flow pattern (Zhu *et al.*, 2007; Uzi and Levy, 2018). The appearance of arches, blockages, erosion or other undesirable phenomena are affected by several parameters related to fluid and particle dynamics or by the pipe geometry, which makes pertinent the development of

models that can better predict these assorted operational setups.

Technological advances have enabled the development of algorithms capable of simulating complex flows computationally. Some conveniences of numerical simulation over experiments are the practicality of changing flow parameters, such as physical properties, the ability of making flow measurements that are not feasible or sometimes even impossible of doing experimentally, and the possibility of investigating critical conditions without risks. However, the reliability of numerical simulations stands upon a good model to describe the system in question. In that sense, particle-fluid flow models are divided in two major groups: treating particles as a continuum media (Euler-Euler) or as a discrete element (Euler-Lagrange) (Zhou *et al.*, 2010). The latter is widely used in fluid-solid flows and is based on coupling Conservative equations for fluid phase together with Newton's second law for translation and rotation of each particle, and the appropriate boundary conditions. One well-established numerical Euler-Lagrange model is the coupled CFD-DEM approach (Zhu *et al.*, 2007, 2008; Zhou *et al.*, 2019), which combines Discrete Element Method (DEM), first proposed by Cundall and Strack (1979), with Computational Fluid Dynamics (CFD), used to describe fluid motion. Several studies were developed using the CFD-DEM approach. Because each particle is treated individually, the interest of using this method is the possibility of investigating the particle-particle and particle-wall interactions, computing the magnitude of contact forces, calculating the frequency of contact or even tracking particles path along the tube, which can be useful in wear calculation or predicting the formation of stable arches/blockages (Xu *et al.*, 2016; Vieira *et al.*, 2016; Duarte *et al.*, 2020; Mondal *et al.*, 2016).

The numerical Euler-Lagrange approach can also be separated in two distinct groups: the unresolved approach and the resolved one. The former is founded on using locally averaged Navier-Stokes equations for the fluid and correlations to describe fluid-particle interactions like drag and lift forces. The latter makes the coupling between fluid and solid by actually computing the flow around each particle. Not only this approach does not rely on correlations and their range of applicability, but also makes possible to use the CFD-DEM method when particles are bigger than computational mesh. Such scenarios can occur when large particles in comparison to pipe dimension are used or when the flow requires a refined CFD mesh (Mondal *et al.*, 2016).

The main objective of this work is to investigate the hydraulic transport of solid particles through a narrow elbow pipe, using a resolved method in the coupled CFD-DEM open-source code CFDEM (Hager *et al.*, 2012) that combines two open-source software packages: LIGGGHTS and OpenFOAM (Goniva *et al.*, 2010). The goal is to examine how the fluid velocity and the particle concentration affects the formation of plugs, clogging or other patterns.

2. MODEL DESCRIPTION

2.1 Solid Phase

The Discrete Element Method (DEM) proposed by (Cundall and Strack, 1979) treats each particle in a Lagrangian framework. The particles are modeled as spheres and can execute two types of motion, translation and rotation, thus their motion are explicitly given by solving Newton's second law. For a particle i with radius r_i, the equations of motion, following Kloss *et al.* (2012), are:

$$m_i \frac{d^2 \boldsymbol{x_i}}{dt^2} = \sum_j (\boldsymbol{F}_{ij}^{cn} + \boldsymbol{F}_{ij}^{ct}) + \boldsymbol{F}_i^f + \boldsymbol{F}_i^b \tag{1}$$

$$I_i \frac{d\boldsymbol{\omega_i}}{dt} = \sum_j \boldsymbol{r_i} \times \boldsymbol{F}_{ij}^{ct} \tag{2}$$

where $\boldsymbol{x}_i$ is the linear position vector and $\boldsymbol{\omega}_i$ is the angular velocity. m_i is the mass and I_i is the moment of inertia. $\boldsymbol{F}_{ij}^{cn}$ and $\boldsymbol{F}_{ij}^{ct}$ are, respectively, the normal and tangential contact forces between particle i and particle or wall j. $\boldsymbol{F}_i^f$ is the force that fluid exerts on the particle. $\boldsymbol{F}_i^b$ is the body forces, which in this case will be considered only due to gravity. In this work, particles are spherical and cohesionless.

In DEM, the contact between particles is usually represented by an overlap between two bodies. The forces acting in this region can be decomposed in a normal and a tangential components with respect to contact surface. Since Cundall and Strack (1979), numerous studies were conducted in this area to develop models for this forces and a good review can be found in Zhu *et al.* (2007).

The contact force model consists of a spring and a dashpot. The spring accounts for the deformation of particle in shock and the dashpot accounts for energy dissipation. It should be noted that the tangential force has an upper boundary equals Coulomb friction force, otherwise the particle would always slip over other solid surfaces. Normal and tangential contact forces between particles i and j can be decomposed as (Kloss *et al.*, 2012):

$$\boldsymbol{F}_{ij}^{cn} = -k_n \boldsymbol{\delta}_n + c_n \Delta \boldsymbol{u}_n \tag{3}$$

$$\boldsymbol{F}_{ij}^{ct} = k_t \int_{t_0}^{t} \Delta \boldsymbol{u}_t \, dt + c_t \Delta \boldsymbol{u}_t \tag{4}$$

where k_n and k_t are, respectively, the normal and tangential stiffness constant. c_n and c_t are, respectively, the normal and tangential damping constant. $\Delta \boldsymbol{u}_n$ and $\Delta \boldsymbol{u}_t$ are the normal and tangential relative velocities between the particles. δ_n is the normal overlap. t_0 is the time when the contact occurs and t when it ends.

By changing the coefficients of stiffness and damping it is possible to change the contact model implemented (Kloss *et al.*, 2012). The contact forces in this work will be modeled following the Hertz-Mindlin and Deresiewicz model (Di Renzo and Di Maio, 2004).

2.2 Fluid Phase

The fluid motion is computed in an Eulerian frame. Therefore, the equations that govern its motion is the incompressible Navier-Stokes with appropriate boundary and initial conditions. The algorithm used by OpenFOAM is based on Finite Volume Method (FVM), so the fluid domain must be discretized in small volumes. In this work it will be used a resolved approach, where the fluid flow is actually computed around the particle and their interactions come directly by solving Navier-Stokes equations. This method is suitable in cases where the particle size overcomes that of mesh cell (Mondal *et al.*, 2016). The resolved approach used is the immersed boundary method which is based on the fictitious domain method presented by Patankar *et al.* (2000). In this method, only one pressure and velocity field exists and the regions covered by particles (Ω_s) are imposed to move as the particle itself, *i.e.* describing a rigid body motion. Following Shirgaonkar *et al.* (2009), the governing equations are:

$$\rho_f \left(\frac{\partial \boldsymbol{u}_f}{\partial t} + \boldsymbol{u}_f \cdot \boldsymbol{\nabla} \boldsymbol{u}_f \right) = \boldsymbol{\nabla} \cdot \boldsymbol{\sigma} \qquad \text{in } \Omega_f \tag{5}$$

$$\nabla \cdot \boldsymbol{u}_f = 0 \qquad \text{in } \Omega_f \tag{6}$$

With initial conditions:

$$\boldsymbol{u}_f(\boldsymbol{x}, t = 0) = \boldsymbol{u}_0 \qquad \text{in } \Omega_f \tag{7}$$

Boundary conditions:

$$\boldsymbol{u}_f = \boldsymbol{u}_\Gamma \qquad \text{on } \Gamma \tag{8}$$

And solid-fluid interface conditions:

$$\boldsymbol{u}_f = \boldsymbol{u}_s \qquad \text{on } \Gamma_s \tag{9}$$

$$\boldsymbol{\sigma} \cdot \boldsymbol{n} = \boldsymbol{t} \qquad \text{on } \Gamma_s \tag{10}$$

where, Ω_f and Ω_s are the domain represented, respectively, by fluid and solid phase. Γ is the fluid boundary and Γ_s the interface between solid and fluid. $\boldsymbol{u}_f$ is the fluid velocity, $\boldsymbol{u}_s$ is the solid velocity, $\boldsymbol{u}_\Gamma$ is the boundary velocity condition for the fluid, $\boldsymbol{u}_0$ is the initial fluid velocity condition, $\boldsymbol{\sigma}$ is the stress tensor, $\boldsymbol{n}$ is a vector pointing outwards solid interface and $\boldsymbol{t}$ is the traction vector due to fluid acting on solid surface.

The algorithm presented in Shirgaonkar *et al.* (2009) to account for fluid motions and its interaction with solid phase is divided in three major steps. The first one is solving equations of motion in the entire domain ($\Omega_f + \Omega_s$) based on previous time-step solutions or initial conditions, neglecting solid phase. The latter will provide an intermediate solution for velocity and pressure fields. The second step is impelling the velocity field inside solid domain (Ω_s) to match the translation and rotation of the solid phase, *i.e.* the fluid inside solid domain will move as a rigid body. This is equivalent to adding a force term in Eq. (5). The third step is to assure velocity continuity at solid-fluid interface, which is done by introducing a scalar field that guarantees divergence-free condition. The force acting on particles is given by integrating the stress tensor inside solid domain:

$$\int \boldsymbol{\nabla} \cdot \boldsymbol{\sigma}(x, y, z, t) \, dV \qquad \text{in } \Omega_s \tag{11}$$

where the stress tensor consists of viscous and pressure terms, which gives a force by unit of volume as in Eq. (12).

$$\boldsymbol{\nabla} \cdot \boldsymbol{\sigma} = -\boldsymbol{\nabla} p + \mu \boldsymbol{\nabla}^2 \boldsymbol{u}_f \tag{12}$$

3. MODEL VALIDATION

The immersed boundary algorithm used in this work, was validated against the sedimentation experiments conducted by Ten Cate *et al.* (2002). The experiment consists in a immersed single sphere settling under gravity in a box. The sphere had a diameter of $d_p = 15\ mm$ and density of $\rho_p = 1120\ kg/m^3$ and was confined in a box with $160\ mm$ height and a square base of $100\ mm$. Three cases were investigated, each one using a different fluid corresponding to cases E1, E3 and E4 presented in Ten Cate *et al.* (2002).

In order to reduce the computational cost, it was previously conducted a mesh validation to check which was the least refined mesh that would still give us accurate results. We found that a good compromise relation between these two quantities could be obtained using a mesh that comprehends an initial refinement of around 2.5 control volumes per particle diameter. Besides, in this work, we make use of a meshing utility from OpenFOAM that performs dynamic grid refinements around each particle as they move inside the domain. This approach also reduces considerably the computational cost, and keeps the calculation accurate near the solid regions.

Figure 1 shows the sphere trajectory and sedimentation velocity obtained with the numerical simulations for the three cases, compared to the experimental results from (Ten Cate *et al.*, 2002). The results obtained in this work are in good agreement with experimental results of Ten Cate *et al.* (2002).

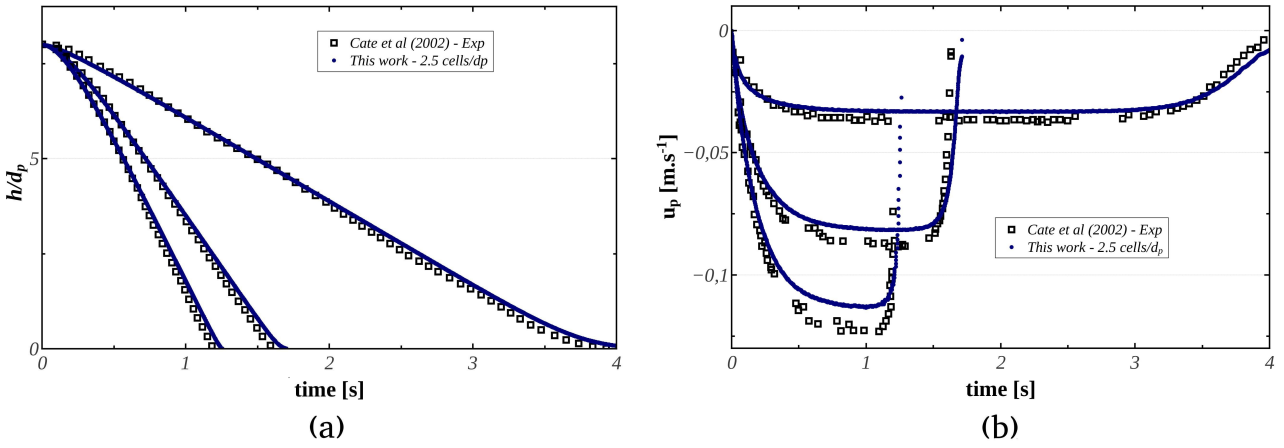

Figure 1. Comparison between numerical simulation of this work with experiments of Ten Cate *et al.* (2002): (a) sphere trajectory; (b) sedimentation velocity

4. SIMULATION SETUP

The simulations were conducted in a pipe, initially filled with water, with $D = 25.4\ mm$ internal diameter. The geometry is constituted of a horizontal section, a $90°$ bend and a vertical section, as depicted in Fig. 2. The vertical section has a length of $5D$, the horizontal of $3D$ and the elbow has a radius of curvature of $2D$. Figure 2 shows the side and front of the initial mesh used in simulation, which are afterward refined during the simulation using the OpenFOAM dynamic mesh utility aforementioned. The initial mesh consisted of 5940 hexahedral elements. At the inlet, located at the horizontal section face, we impose a constant velocity of $\bar{U} = 0.12\ m/s$, which yields to a Reynolds number of 3048. Although we are considering a flow in a turbulent transition, because of the fluid confinement due to the size of the particles, we assumed a laminar flow regime for sake of simplicity. The outlet is at the vertical section face, where a zero-gradient condition for the velocity was considered. For the pipe walls we used a no-slip condition for the fluid, and for the pressure, a zero-gradient at the inlet and a fixed value at the outlet were employed. The gravity points downwards. Table 1 summarizes fluid properties used in simulations.

The simulation was initialized with a few particles inside the domain. The subsequent particles were generated in aleatory positions at an insertion box outside the domain and they entered at a constant mass rate of $0.008\ kg/s$ with the same velocity of the fluid, in order to reduce flow perturbations. Particle properties were chosen to represent Nylon 6,6 and are described in Tab.1. It is important to highlight that the Young's Modulus used in simulations was in fact two orders of magnitude lower than the one in Tab. 1, because it allowed us to use a higher time-step in DEM and still capture the main features of the flow Mondal *et al.* (2016).

The DEM time-step should be small enough to consider the collision time span. For the CFD it is recommended for accurate solutions when using immersed boundary method that the coupling CFD-DEM time-steps should be around 10 to 50 times the DEM time-step. Here, the time-step used in CFD and DEM were, respectively, $1 \times 10^{-4}\ s$ and $2 \times 10^{-5}\ s$. The PISO (pressure-implicit with splitting of operators) algorithm was used to solve fluid flow equations. The discretizations schemes used was Euler for time derivatives and Gauss linear for spatial derivatives.

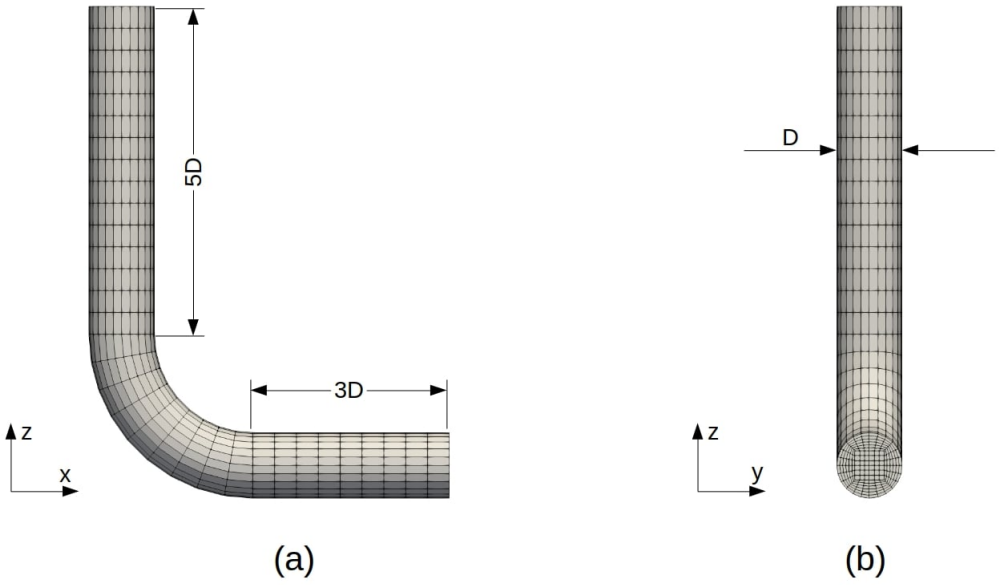

Figure 2. Computational mesh and domain dimensions: (a) side view; (b) front view

Table 1. Parameters used in simulation.

Particle diameter d (mm)	6
Particle density ρ_s (kg/m^3)	1140
Young's Modulus E (GPa)	3.3
Poisson's ratio ν	0.41
Restitution coefficient e	0.5
Coefficient of friction μ	0.25
Fluid density ρ_f (kg/m^3)	1000
Fluid dynamic viscosity μ_f ($Pa \cdot s$)	1×10^{-3}

5. PRELIMINARY RESULTS

First, we performed a single phase simulation to check the fluid flow inside the pipe and the validity of the initial and boundary conditions. The fluid properties and flow initial and boundary conditions are the same as those used in the two-phase simulation. Figure 3 depicts the pressure distribution, the streamlines of the flow and the velocity field. Those results are consistent with the ones found in the literature (Xu *et al.*, 2016), showing a low pressure in the convex wall of the elbow and a high pressure in the concave wall. It should be noted that, because the flow is incompressible, OpenFOAM calculates the pressure divided by fluid density and the value adopted is arbitrary, for only pressure gradient is significant. It is noticeable that the fluid accelerates in the leftmost region of the vertical section.

Figure 4 shows snapshots of particle positions at the firsts 5 seconds of simulation.

As the particles move upwards, they describe a swirl motion, characteristic of the secondary flow in a $90°$ elbow, due to an imbalance of centrifugal forces and pressure gradient (Kim *et al.*, 2014). Investigations regarding the influence of the rate of particle insertion and fluid velocity are being carried out.

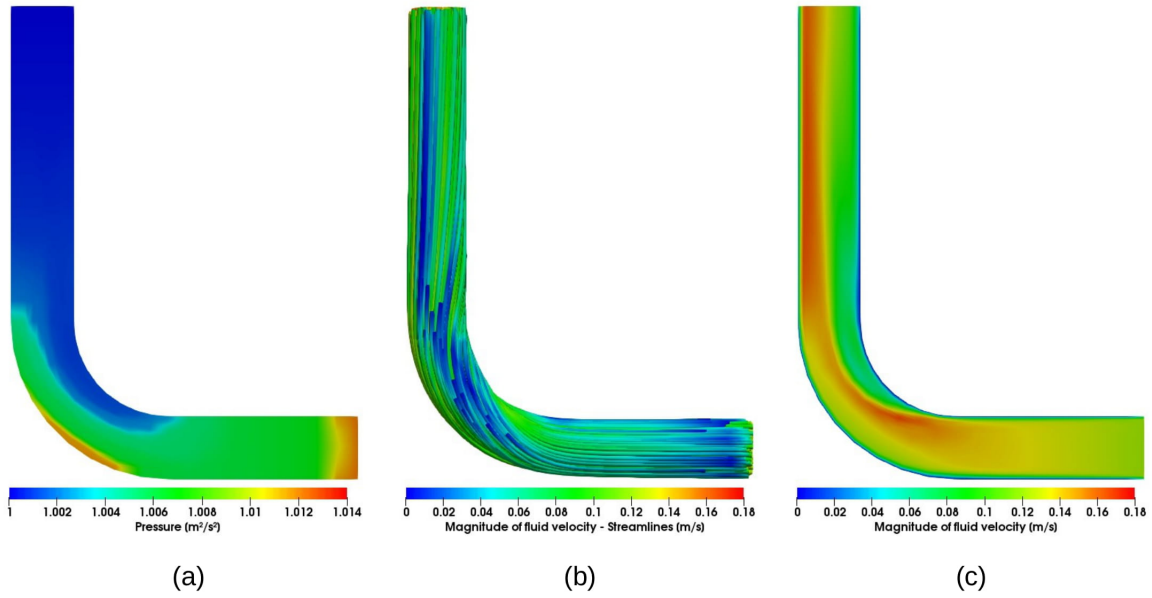

Figure 3. (a) fluid pressure; (b) streamlines showing the magnitude of fluid velocity; (c) magnitude of fluid velocity

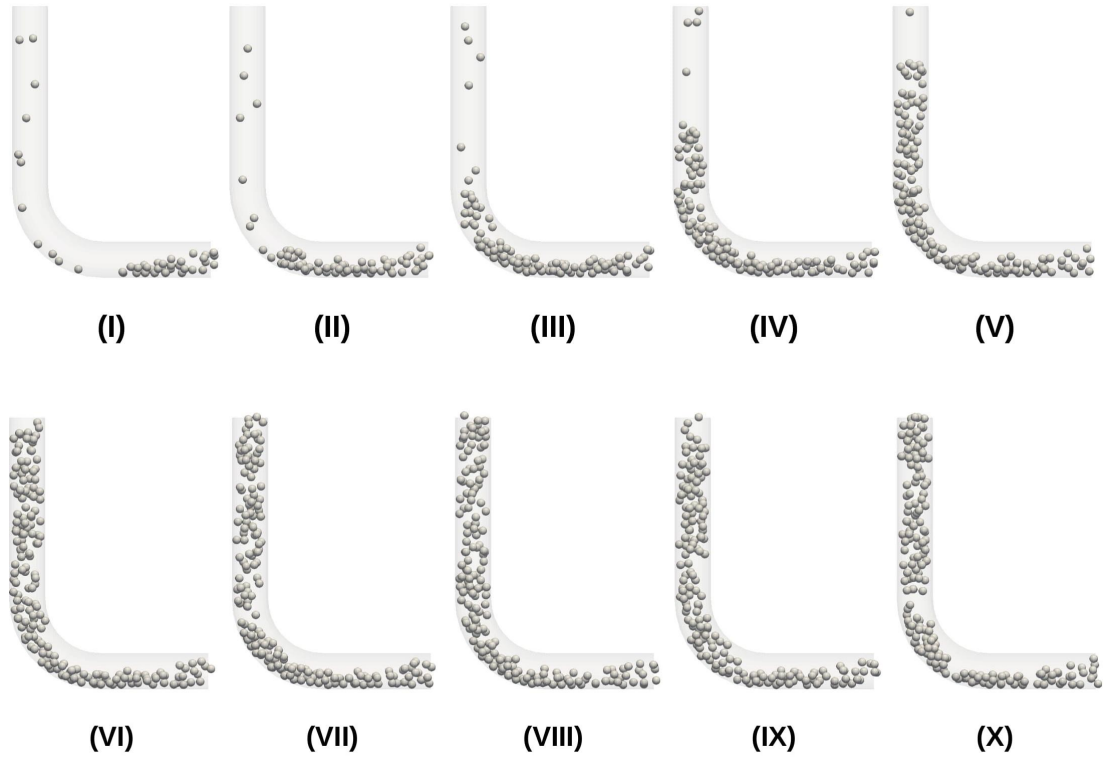

Figure 4. Particles position in X-Z plane at: (I) $0.5s$; (II) $1.0s$; (III) $1.5s$; (IV) $2.0s$; (V) $2.5s$; (VI) $3.0s$; (VII) $3.5s$; (VIII) $4.0s$; (IX) $4.5s$; (X) $5.0s$

6. ACKNOWLEDGEMENTS

The authors would like to thank the National Council for Scientific and Technological Development - CNPq (Grant No. 144544/2019-9) and the São Paulo Research Foundation - FAPESP (Grant. Nos. 2018/14981-7 and 2019/20888-2) for the financial support provided.

7. REFERENCES

Cundall, P.A. and Strack, O.D., 1979. "A discrete numerical model for granular assemblies". *geotechnique*, Vol. 29, No. 1, pp. 47–65.

Di Renzo, A. and Di Maio, F.P., 2004. "Comparison of contact-force models for the simulation of collisions in dem-based granular flow codes". *Chemical engineering science*, Vol. 59, No. 3, pp. 525–541.

Duarte, C.A.R., de Souza, F.J., Venturi, D.N. and Sommerfeld, M., 2020. "A numerical assessment of two geometries for reducing elbow erosion". *Particuology*, Vol. 49, pp. 117–133.

Duran, J., 2012. *Sands, powders, and grains: an introduction to the physics of granular materials*. Springer Science & Business Media.

Goniva, C., Kloss, C., Hager, A. and Pirker, S., 2010. "An open source cfd-dem perspective". In *Proceedings of OpenFOAM Workshop, Göteborg*. pp. 22–24.

Hager, A., Kloss, C., Pirker, S. and Goniva, C., 2012. "Parallel open source cfd-dem for resolved particle-fluid interaction". In *Proceedings of 9th International Conference on Computational Fluid Dynamics in Minerals and Process Industries*. pp. 1–6.

Kim, J., Yadav, M. and Kim, S., 2014. "Characteristics of secondary flow induced by 90-degree elbow in turbulent pipe flow". *Engineering Applications of Computational Fluid Mechanics*, Vol. 8, No. 2, pp. 229–239.

Kloss, C., Goniva, C., Hager, A., Amberger, S. and Pirker, S., 2012. "Models, algorithms and validation for opensource dem and cfd–dem". *Progress in Computational Fluid Dynamics, an International Journal*, Vol. 12, No. 2-3, pp. 140–152.

Li, Y., Zhang, H., Lin, Z., He, Z., Xiang, J. and Su, X., 2019. "Relationship between wear formation and large-particle motion in a pipe bend". *Royal Society open science*, Vol. 6, No. 1, p. 181254.

Mondal, S., Wu, C.H. and Sharma, M.M., 2016. "Coupled cfd-dem simulation of hydrodynamic bridging at constrictions". *International Journal of Multiphase Flow*, Vol. 84, pp. 245–263.

Parry, A. and Millet, O., 2010. "Modeling blockage of particles in conduit constrictions: dense granular-suspension flow". *Journal of fluids engineering*, Vol. 132, No. 1.

Parsi, M., Najmi, K., Najafifard, F., Hassani, S., McLaury, B.S. and Shirazi, S.A., 2014. "A comprehensive review of solid particle erosion modeling for oil and gas wells and pipelines applications". *Journal of Natural Gas Science and Engineering*, Vol. 21, pp. 850–873.

Patankar, N.A., Singh, P., Joseph, D.D., Glowinski, R. and Pan, T.W., 2000. "A new formulation of the distributed lagrange multiplier/fictitious domain method for particulate flows". *International Journal of Multiphase Flow*, Vol. 26, No. 9, pp. 1509–1524.

Shirgaonkar, A.A., MacIver, M.A. and Patankar, N.A., 2009. "A new mathematical formulation and fast algorithm for fully resolved simulation of self-propulsion". *Journal of Computational Physics*, Vol. 228, No. 7, pp. 2366–2390.

Ten Cate, A., Nieuwstad, C., Derksen, J. and Van den Akker, H., 2002. "Particle imaging velocimetry experiments and lattice-boltzmann simulations on a single sphere settling under gravity". *Physics of Fluids*, Vol. 14, No. 11, pp. 4012–4025.

Uzi, A. and Levy, A., 2018. "Flow characteristics of coarse particles in horizontal hydraulic conveying". *Powder Technology*, Vol. 326, pp. 302–321.

Vaezi, M., Verma, S. and Kumar, A., 2018. "Application of high-frequency impedancemetry approach in measuring the deposition velocities of biomass and sand slurry flows in pipelines". *Chemical Engineering Research and Design*, Vol. 140, pp. 142–154.

Vieira, R.E., Mansouri, A., McLaury, B.S. and Shirazi, S.A., 2016. "Experimental and computational study of erosion in elbows due to sand particles in air flow". *Powder technology*, Vol. 288, pp. 339–353.

Xu, L., Zhang, Q., Zheng, J. and Zhao, Y., 2016. "Numerical prediction of erosion in elbow based on cfd-dem simulation". *Powder Technology*, Vol. 302, pp. 236–246.

Zhou, M., Wang, S., Kuang, S., Luo, K., Fan, J. and Yu, A., 2019. "Cfd-dem modelling of hydraulic conveying of solid particles in a vertical pipe". *Powder Technology*, Vol. 354, pp. 893–905.

Zhou, Z., Kuang, S., Chu, K. and Yu, A., 2010. "Discrete particle simulation of particle–fluid flow: model formulations and their applicability". *Journal of Fluid Mechanics*, Vol. 661, pp. 482–510.

Zhu, H., Zhou, Z., Yang, R. and Yu, A., 2007. "Discrete particle simulation of particulate systems: theoretical developments". *Chemical Engineering Science*, Vol. 62, No. 13, pp. 3378–3396.

Zhu, H., Zhou, Z., Yang, R. and Yu, A., 2008. "Discrete particle simulation of particulate systems: a review of major applications and findings". *Chemical Engineering Science*, Vol. 63, No. 23, pp. 5728–5770.

8. RESPONSIBILITY NOTICE

The author(s) is (are) solely responsible for the printed material included in this paper.